

## Evaporation-driven clustering of microscale pillars and lamellae

Tae-Hong Kim, Jungchul Kim, and Ho-Young Kim

Citation: *Physics of Fluids* **28**, 022003 (2016); doi: 10.1063/1.4941083

View online: <http://dx.doi.org/10.1063/1.4941083>

View Table of Contents: <http://scitation.aip.org/content/aip/journal/pof2/28/2?ver=pdfcov>

Published by the [AIP Publishing](#)

---

### Articles you may be interested in

[Evaporation-driven low Reynolds number vortices in a cavity](#)

*Phys. Fluids* **26**, 033102 (2014); 10.1063/1.4868546

[Charge-pumping in a synthetic leaf for harvesting energy from evaporation-driven flows](#)

*Appl. Phys. Lett.* **95**, 013705 (2009); 10.1063/1.3157144

[Adhesion at interfaces between highly entangled polymer melts](#)

*J. Rheol.* **52**, 749 (2008); 10.1122/1.2901231

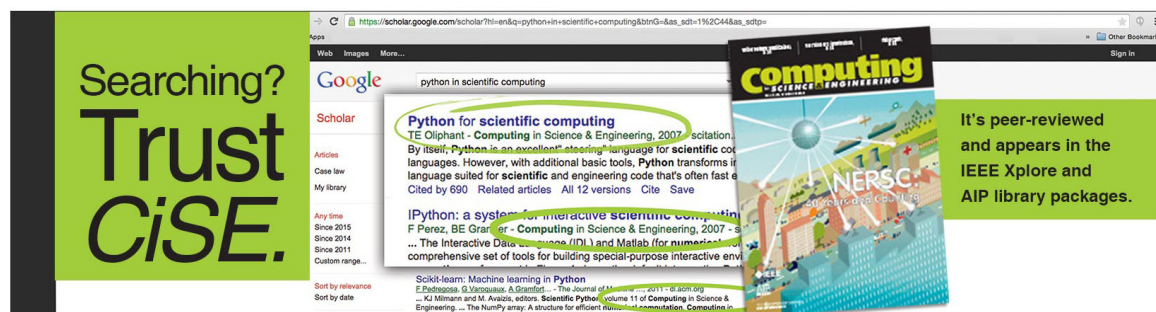
[Flow of evaporating, gravity-driven thin liquid films over topography](#)

*Phys. Fluids* **18**, 013601 (2006); 10.1063/1.2148993

[Control of evaporatively driven instabilities of thin liquid films](#)

*Phys. Fluids* **14**, 1895 (2002); 10.1063/1.1476304

---

A composite image featuring a green banner on the left with the text 'Searching? Trust CiSE.' in white. In the center is a screenshot of a Google Scholar search for 'python in scientific computing'. The search results show a top entry for 'Python for scientific computing' by J.E. Olliphant, with a citation and a brief description. Below it is another entry for 'IPython: a system for interactive scientific computing'. To the right of the search results is a book cover for 'Computing in Science & Engineering' by NERSC, featuring a colorful, abstract design. On the far right, a green box contains the text: 'It's peer-reviewed and appears in the IEEE Xplore and AIP library packages.'

# Evaporation-driven clustering of microscale pillars and lamellae

Tae-Hong Kim, Jungchul Kim, and Ho-Young Kim<sup>a)</sup>

*Department of Mechanical and Aerospace Engineering, Seoul National University, Seoul 08826, South Korea*

(Received 4 July 2015; accepted 19 January 2016; published online 8 February 2016)

As a liquid film covering an array of micro- or nanoscale pillars or lamellae evaporates, its meniscus pulls the elastic patterns together because of capillary effects, leading to clustering of the slender microstructures. While this elasto-capillary coalescence may imply various useful applications, it is detrimental to a semiconductor manufacturing process called the spin drying, where a liquid film rinses patterned wafers until drying. To understand the transient mechanism underlying such self-organization during and after liquid evaporation, we visualize the clustering dynamics of polymer micropatterns. Our visualization experiments reveal that the patterns clumped during liquid evaporation can be re-separated when completely dried in some cases. This restoration behavior is explained by considering adhesion energy of the patterns as well as capillary forces, which leads to a regime map to predict whether permanent stiction would occur. This work does not only extend our understanding of micropattern stiction, but also suggests a novel path to control and prevent pattern clustering. © 2016 AIP Publishing LLC. [<http://dx.doi.org/10.1063/1.4941083>]

## I. INTRODUCTION

When thin and flexible solid structures like pillars and lamellae are brought into contact with a liquid-air interface, the structures may deform as pulled by capillary forces.<sup>1-3</sup> Such interaction between elastic and capillary forces, termed elastocapillarity, can be utilized to manipulate the geometry of thin sheets through capillary origami<sup>4</sup> or wrinkling,<sup>5,6</sup> to control the supporting forces of floating objects,<sup>7-9</sup> and to actuate micromechanical systems.<sup>10</sup> Complex hierarchical structures can be fabricated through the so-called elastocapillary coalescence,<sup>11-16</sup> which relies on the capillarity-induced adhesion and clumping of flexible micro- and nanostructures.

The coalescence of fine patterns is, however, detrimental to manufacturing of semiconductor chips with extremely fragile patterns of ever-shrinking sizes. Collapse of microstructures under the influence of rinsing liquids, often referred to as stiction, has been reported since decades ago.<sup>17-19</sup> In the current manufacturing process of integrated circuit chips with nanoscale features, the coalescence of high-aspect-ratio structures is reported to occur mainly in the spin-drying step, in which a rinsing liquid covering a wafer is rapidly dried to remove residues of cleaning solutions.<sup>16</sup> Preventing the clustering of nanostructures in the chip has now become a critical technological challenge to keep a high production yield.<sup>17,20</sup>

The majority of previous studies has been focused on the role of capillary forces that overcome the elastic resistance of the structures to pull them together.<sup>21,22</sup> We also start our theoretical discussion by comparing the capillary and elastic forces to explain the clumping of microstructures during liquid evaporation. However, our experiments to image the transient process of microstructure deformation, which was hardly reported before, allows us to go beyond this force argument. It is revealed that some patterns clumped during liquid evaporation are re-separated when completely dried, leading us to consider energy states of the final configuration. Furthermore, we show that

<sup>a)</sup>Electronic address: [hyk@snu.ac.kr](mailto:hyk@snu.ac.kr)

in practical situations where the arrays of pillars and lamellae are dried, the liquid dries from the bottom first rather than the top because the gap closes at the top. Our experimental approach and consideration of energy states of the clumped system leads to regime maps that can predict whether microstructures would ever touch each other and then remain stuck together.

## II. EXPERIMENTAL

Figure 1(a) shows an experimental setup used to observe the interaction between an evaporating film and microstructures during the drying process. Microscale arrays of pillars and lamellae, whose SEM (scanning electron microscopy) images are shown in Figs. 1(b) and 1(c), respectively, are fabricated by soft lithography<sup>23</sup> using the mixture of PDMS (polydimethylsiloxane) prepolymer base and the curing agent in a weight ratio of 10:1. The mixture is poured onto a negative patterned silicon master prepared by deep reactive ion etching and treated with an antisticking agent (octafluorocyclobutane,  $C_4F_8$ ), and degassed under vacuum for 1 h to eliminate air bubbles. Curing is carried out at 80 °C for 1 h in an oven, and the PDMS array is peeled off from the silicon master. The cylindrical pillars in the square array have the diameter  $d$  and the side-to-side spacing  $s$ , and  $d = s = 10 \mu\text{m}$ . In the arrays of lamellae, the thickness  $c$  and the gap  $b$  are identically  $10 \mu\text{m}$  and the width  $w$  is  $50 \mu\text{m}$ . The height of the pillars and lamellae,  $h$ , ranges from 20 to  $40 \mu\text{m}$ , so that the aspect ratio defined as  $\eta = h/d$  and  $h/c$  for pillars and lamellae, respectively, varies from 2 to 4.

As the liquids covering the PDMS array, we use de-ionized water, IPA (isopropyl alcohol, Sigma-Aldrich) and HFE-7100 (methoxy-nonafluorobutane, 3M Novec), of which IPA and HFE-7100 are widely used for wafer cleaning. The surface tension coefficient, the contact angle with PDMS, and boiling point of the liquids are listed in Table I. Pristine PDMS patterns are used with

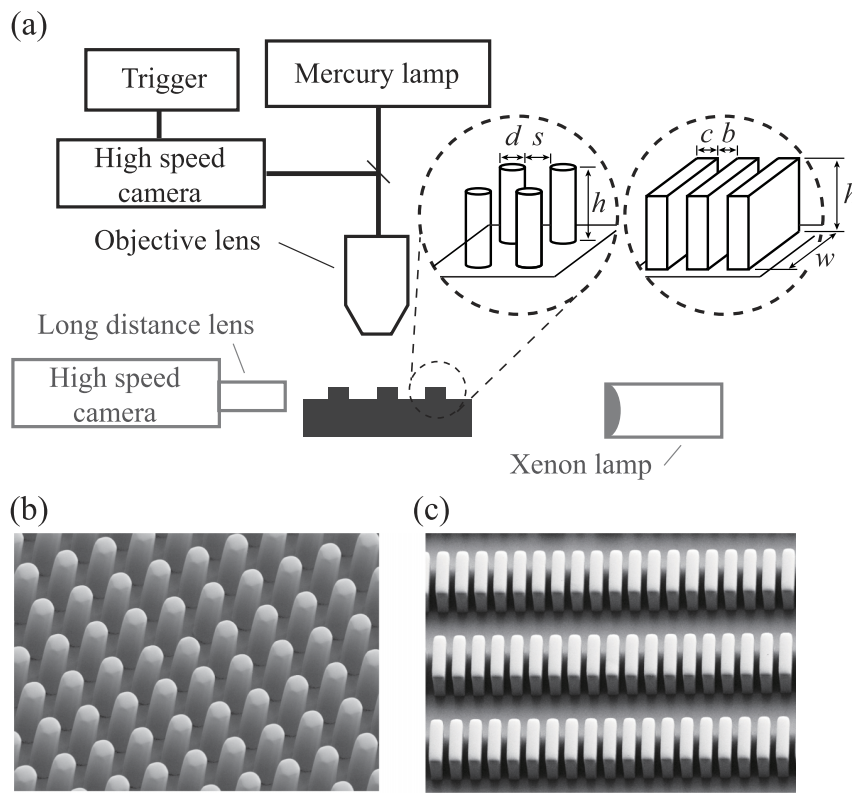


FIG. 1. (a) Experimental apparatus to image the liquid film behavior leading to pattern collapse. The high-speed camera is situated either horizontally (drawn in grey) or vertically (drawn in black) to take the side or top view. The insets depict the dimensions of the arrays of cylindrical pillars and lamellae. SEM images of the arrays of (b) cylindrical pillars and (c) lamellae. Scale bars,  $50 \mu\text{m}$ .

TABLE I. Properties of liquids; surface tension coefficient at 25°C, boiling point at 1 atm, and contact angle on a flat PDMS surface.

Liquid	Surface tension (mN m <sup>-1</sup> )	Boiling point (°C)	Contact angle (deg)
IPA	22.4	82.5	22
HFE-7100	13.6	61	~0
Water	72.0	100.0	~5 (air plasma treated)

the low-surface-tension liquids, IPA and HFE-7100, while PDMS patterns are hydrophilized by 5 min of air plasma treatment before deposition of water. The experiments are carried out under the ambient conditions of temperature 25 °C and humidity 30%. The high-speed camera (Photron SA1.1) is either aligned horizontally with the array to take its side view, or mounted on an upright microscope (Olympus BX-51M) to take the top view.

### III. OBSERVATIONS OF MICROPATTERN CLUSTERING

Figure 2 (Multimedia view) displays various images of micropattern clustering due to liquid evaporation. As shown in Fig. 2(a), the nucleation of a pillar bundle occurs at a random site near time  $t = 0$  s. This happens when the liquid evaporates to the level of the free tips, to form a meniscus connecting neighboring pillars. Imperfections and instabilities, which include local differences in the evaporation rate, pinning of the contact line, and variations in the spacing nucleate the first pillar cluster. As a result, the next pillar senses an anisotropic force field and bends. This process propagates through the pillars, generating long-range ordered areas as shown at  $t = 39.75$  s.

Figures 2(b) and 2(c) (Multimedia view) show the clustering of lamellae. The side-view images of Fig. 2(c) (Multimedia view) show the process starting with the meniscus being caught at the tips of lamellae ( $t = 0$  s). Subsequently, the forces due to surface tension pull the patterns asymmetrically because of inherent nonuniformity of the pattern spacing,<sup>14</sup> or small film disturbances caused by nonuniform evaporation rates. In Fig. 2(c) (Multimedia view), the symmetry of meniscus heights or gap widths is broken as shown in the second panel (0.12 s). The difference of the gap widths grows, which in turn aggravates nonuniformity of evaporation rates. Thus, the liquid height becomes progressively more nonuniform as shown in the third (0.37 s) and fourth (0.65 s) panels. The gap filled with liquid is subject to the pressure lower than the atmospheric pressure because of surface tension effects. Therefore, the patterns separated by liquid-filled gaps are brought together and lean against each other. As evaporation continues (between 0.65 and 0.80 s), the liquid that used to fill the gaps between the patterns deforming apart from each other is completely dried. In the gaps between the clustering patterns, the base is dried first because the gap closes at the top with the liquid at the upper portion preserved longer. The lower meniscus rises up reducing the volume of the drop confined within the gap. The patterns appear stuck together as the liquid film almost disappears from the gap, as shown in the last panel (1.03 s). This may lead to permanent adhesion of the patterns unless they are restored later. Figures 2(d) and 2(e) show the SEM images of the clustered arrays of pillars and lamellae, respectively, after complete evaporation of liquid.

### IV. THEORETICAL CONSIDERATIONS

We theoretically consider the conditions that lead the patterns to cluster by comparing the capillary forces to pull the solid structures together and the elastic resistance to bending. We then discuss the final states reached by the clumped patterns, which are determined by the adhesion energy of the solid surfaces.

#### A. Conditions for contact

When the left-right symmetry is broken, the lamellae are pulled together by the surface tension force acting along the contact line and the pressure force on the wetted area as shown in Fig. 3(a).

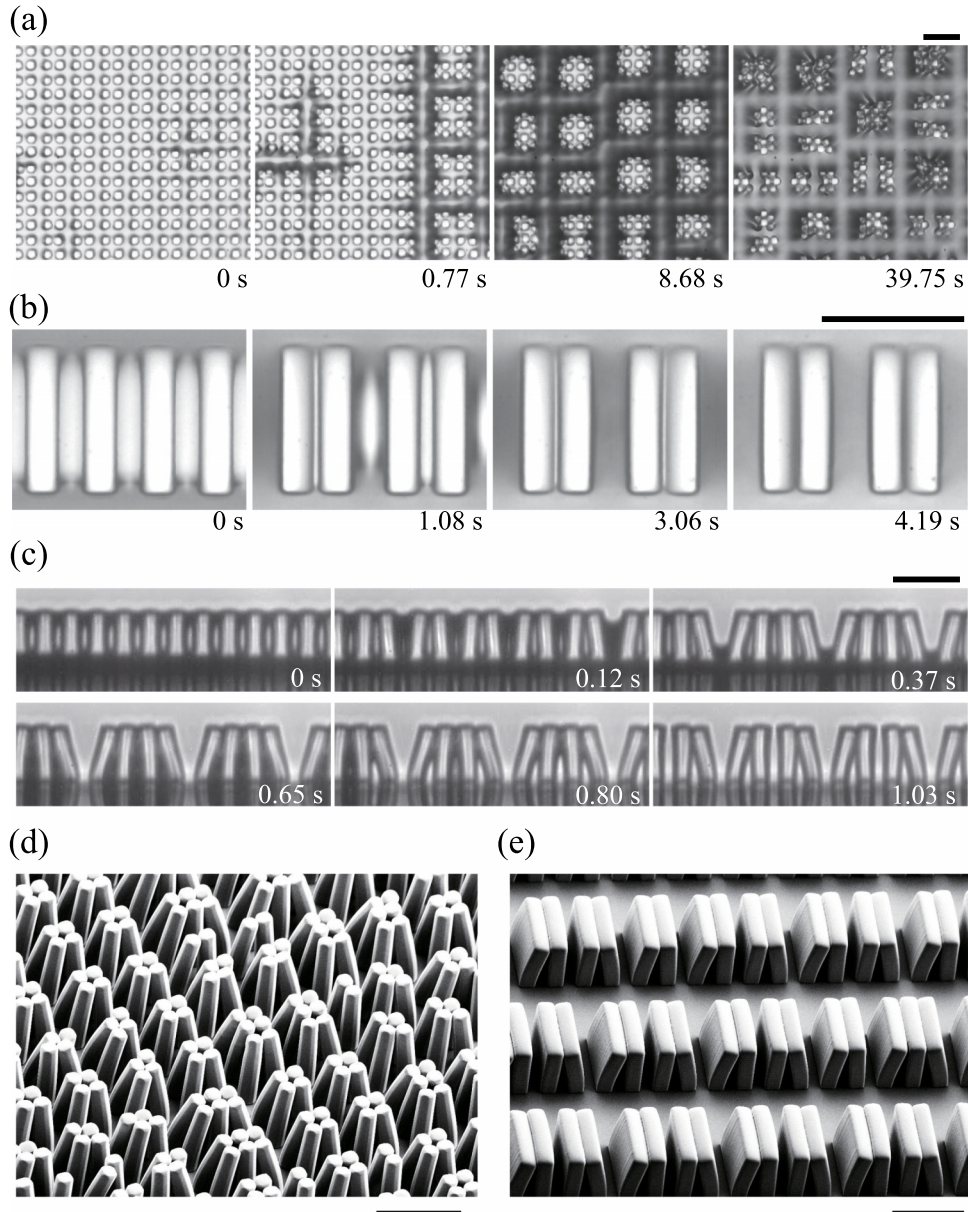


FIG. 2. Clustering micropatterns. Arrays of pillars and lamellae of the aspect ratio 4 are bundled with the evaporation of IPA. Top views of the arrays of (a) cylindrical pillars and (b) lamellae. (c) Side view of the array of lamellae. SEM images of the arrays of (d) cylindrical pillars and (e) lamellae. Scale bars, 50  $\mu\text{m}$ . (Multimedia view) [URL: <http://dx.doi.org/10.1063/1.4941083.1>]

The capillary forces give rise to the torque to bend the patterns, but it is resisted by the flexural rigidity. Here, we consider the competition between the capillary and elastic forces through scaling analysis. For simplicity, we consider the interaction between the pattern surfaces facing the approaching pattern only. It is because the gap between the patterns that are bent away from each other (denoted by A in Fig. 3(a)) dries significantly faster than the gap (B) between clustering patterns.

The bending moment per unit width of a lamella at the clamped end,  $M_b$ , can be scaled as

$$M_b \sim \sigma h \sin \theta + \frac{\sigma h^2 \cos \theta}{b}, \quad (1)$$

where  $\sigma$  is the surface tension coefficient between liquid and air and  $\theta$  is the contact angle of the liquid with the pattern surface. The first term on the right-hand side is due to surface tension which

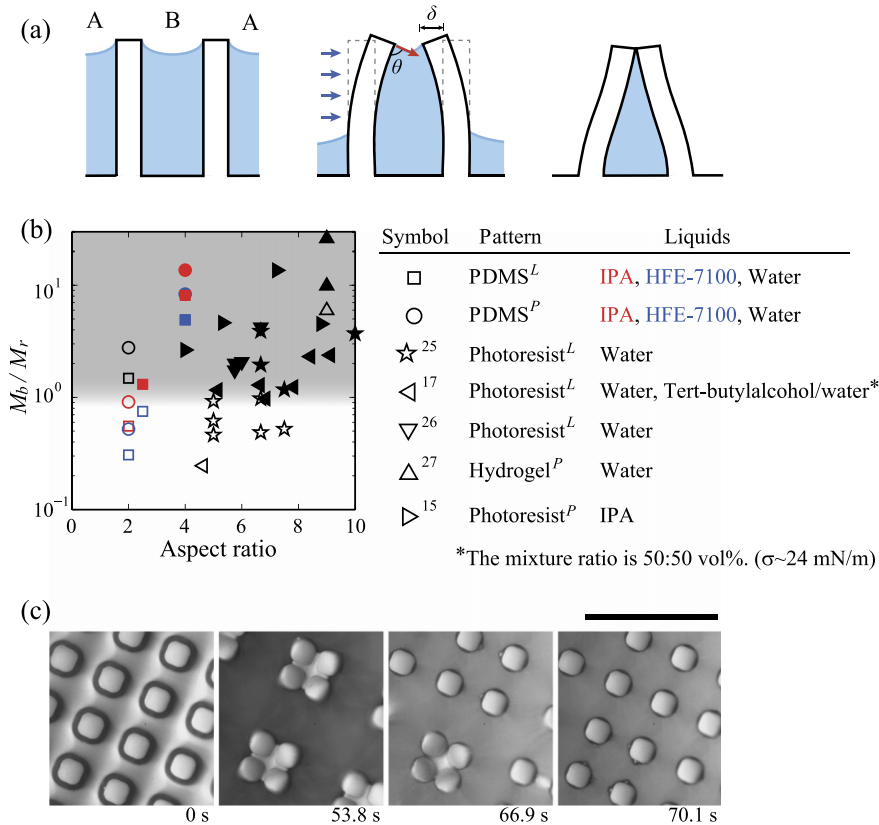


FIG. 3. (a) Forces acting on the lamellae bending due to liquid evaporation. Red arrow indicates the surface tension force and blue arrows correspond to the pressure force. (b) Experimental data indicating the stiction behavior of the pillars plotted using the moment ratio and the aspect ratio. The filled symbols indicate permanent stiction and empty symbols non-stiction. The squares and circles correspond to the results of the present work and the other symbols are from literature. Superscripts *P* and *L* indicate pillars and lamellae, respectively. (c) Top view of the array of cylindrical pillars with the aspect ratio of 2. The tops of the pillars are brought together but eventually separated as the liquid (IPA) disappears with evaporation. Scale bar, 50  $\mu\text{m}$ . (Multimedia view) [URL: <http://dx.doi.org/10.1063/1.4941083.2>]

is a concentrated force operating on the three-phase line, and becomes very small for low contact angles. The second term accounts for the torque due to pressure difference between the dry and wet faces. The dry face of the pillar as shown in the second and third panels in Fig. 3(a) experiences the atmospheric pressure. Whereas, the pressure in the liquid-filled gap is lower than the atmospheric pressure by  $\Delta p = \sigma \kappa$ , where  $\kappa = b/(2 \cos \theta)$  is the curvature of the meniscus. The moment per unit width due to this Laplace pressure is scaled as  $\sim \Delta p h^2$ , which gives the second term in Eq. (1).

The elastic resistance moment acting on the deflected pattern,  $M_r$ , is scaled as<sup>28</sup>

$$M_r \approx \frac{EI\delta}{h^2}, \quad (2)$$

where  $E$  is Young's modulus of the structure,  $I$  is the area moment of inertia per unit width ( $I = c^3/12$ ), and  $\delta$  is the displacement at the free end. The ratio of the capillary bending moment to the elastic resistance moment determines whether the patterns touch each other. When the maximum displacement is half the spacing,  $\delta = b/2$ , the moment ratio becomes  $M_b/M_r \approx 24\sigma(h/c)^4[(c/h) \sin \theta + (c/b) \cos \theta]/(Eb)$ . Our interest lies in whether the capillary effects can keep the pillars clustered until the late stage of evaporation when the contact angle  $\theta$  is low. Thus, the moment ratio can be simply estimated as

$$\frac{M_b}{M_r} \approx 24 \frac{c\sigma \cos \theta}{Eb^2} \eta^4, \quad (3)$$

where  $\eta$  is the aspect ratio,  $h/c$ .

We now consider the case of an array of cylindrical pillars with  $I = \pi d^4/64$ . During the liquid evaporation, capillary forces pull the multiple pillars towards the center of the aggregate as shown in Fig. 2(a). As the pillars tend to bend in a diagonal direction, we get  $\delta \approx \sqrt{2}s/2$ . Therefore, the moment ratio for the cylindrical pillars is estimated as  $M_b/M_r \approx 64\sqrt{2}\sigma(h/d)^4[(d/h)\sin\theta + \sqrt{2}(d/s)\cos\theta]/(\pi Eb)$ . For the late stage where the contact angle is low, the moment ratio is simply given by

$$\frac{M_b}{M_r} \approx \frac{128}{\pi} \frac{d\sigma \cos\theta}{Es^2} \eta^4, \quad (4)$$

where the aspect ratio  $\eta = h/d$ .

The patterns tend to bend and lean against each other when the bending-to-resisting moment ratio is high. Our scaling relations reveal that patterns of a high aspect ratio, narrow spacing, and softer material bend and contact more readily when surrounded by a high surface-tension liquid. In particular, the moment ratio is critically sensitive to the aspect ratio ( $\eta$ ) of the patterns as it is proportional to  $\eta^4$ .

To test this analysis based on force argument, we plot the experimental data indicating whether the micropatterns stick together after complete evaporation of liquid films in the two-dimensional space constructed by the moment ratio and the aspect ratio in Fig. 3(b). The data consist of previously reported ones and those obtained in this work. Table II lists Young's modulus  $E$  and surface energy  $\gamma_s$  of the solids considered. We see that all the data points for  $M_b/M_r$  below  $\sim 10^0$  correspond to non-stiction (empty symbols). However, for  $M_b/M_r$  higher than  $\sim 10^0$ , some data points exhibit permanent stiction (filled symbols) while others not. This indicates that the moment ratio is an insufficient indicator to predict whether the patterns would cluster permanently.

Our visualization results reveal that when  $M_b/M_r \lesssim 10^0$ , the patterns do not bend enough to touch their neighbors as our modeling predicts. When  $M_b/M_r \gtrsim 10^0$ , the microstructures are bent and lean against their neighbors during liquid evaporation. However, as displayed in Fig. 3(c) (Multimedia view), in some conditions pillars that are bundled first are eventually separated as the liquid confined by the gap is completely evaporated. The corresponding points are the empty symbols located above  $M_b/M_r \sim 10^0$  in Fig. 3(b). In other words, merely observing the end states of the pillars after liquid evaporation cannot tell whether the pillars have been bent to touch each other during evaporation. We seek a condition different from the foregoing moment ratio which can predict the permanent stiction of microstructures in the following.

## B. Conditions for permanent adhesion

Although the patterns must be brought into contact while liquid is present for adhesion to occur, it is only a necessary condition for permanent stiction. As demonstrated above, the contact should be maintained even after the array is completely dried. Otherwise, the patterns are separated again, which is actually desirable in some situations including semiconductor manufacturing processes. As

TABLE II. Young's modulus and surface energy in air of the selected materials.<sup>17,25–27,29–31</sup>

Material	Young's modulus (MPa)	Surface energy (mJ m <sup>-2</sup> )
PDMS	1.7	22
Photoresist (SAL 601) <sup>25,26</sup>	$5.9 \times 10^3$	$\sim 50$
Photoresist (AZ-PN 100) <sup>17,26</sup>	$5.9 \times 10^3$	$\sim 50$
Photoresist (PMMA) <sup>15</sup>	$3 \times 10^3$	$\sim 50$
Hydrogel (PHEMA-co-PMMA, 25 wt. %) <sup>27</sup>	20	33
Hydrogel (PHEMA-co-PMMA, 40 wt. %) <sup>27</sup>	74	33
Hydrogel (PHEMA-co-PMMA, 50 wt. %) <sup>27</sup>	158	33
Hydrogel (PHEMA-co-PMMA, 60 wt. %) <sup>27</sup>	274	33
Hydrogel (PHEMA-co-PMMA, 67 wt. %) <sup>27</sup>	724	33
Hydrogel (PHEMA-co-PMMA, 75 wt. %) <sup>27</sup>	1200	33

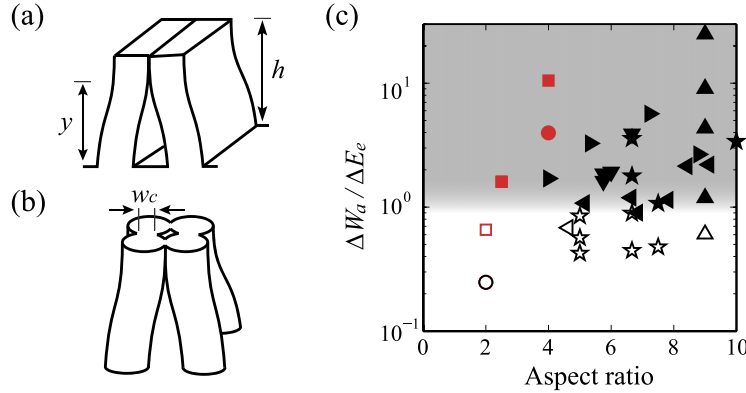


FIG. 4. Permanent adhesion due to surface energy. Schematic models of (a) two lamellae and (b) four cylindrical pillars. (c) Adhesion regime map. The filled symbols indicate stiction and empty symbols non-stiction. The energy change ratio determines whether the adhesion would persist.

the liquid film between the tips of the clumped patterns disappears, the adhesive forces owing to the surface energy of the solid, instead of the capillary forces, must keep the patterns stuck together. Therefore, the final state of the patterns is determined by the competition between the elastic strain energy and adhesive energy between the patterns. A similar idea to predict the stability of elastic systems subject to deflections can be found in the lateral collapse in microcontact printing<sup>32</sup> and replica molding of soft-lithography techniques<sup>33,34</sup> although they do not involve liquid evaporation.

We start with a situation depicted in Fig. 4(a), where two lamellae lean against each other with  $y$  being the height of the non-contact region, so that the contact length is  $h - y$ . The elastic strain energy per unit width stored in the lamellae is scaled as  $E_e \approx E Ib^2 / (4y^3)$ .<sup>28</sup> For the lamellae to restore their straight configurations, the contact length should decrease, or  $y$  should increase. The elastic energy decreases by  $\Delta E_e$  as the non-contact length increases by  $\Delta y$ :  $\Delta E_e \approx 3E Ib^2 \Delta y / (4y^4)$ . As the lamellae become separated, new surfaces are exposed to air. This elevates the total energy of the system per unit width by  $\Delta W_a$ , where  $W_a$  signifies the work of adhesion. By the Dupré equation,  $\Delta W_a = 2\gamma_s \Delta y$ , where  $\gamma_s$  is the surface energy of the solid per unit area.<sup>24</sup> The change of the total energy of the system per unit width associated with the decrease of the contact length can be written as  $\Delta E_t = \Delta W_a - \Delta E_e$ . The lamellae initially clustered can be separated when the system energy decreases, or  $\Delta E_t < 0$ , with the increase of the non-contact length  $\Delta y$ . Therefore, we should get  $\Delta E_e > \Delta W_a$  or  $\Delta W_a / \Delta E_e < 1$  for the lamellae to be separated. The ratio of the adhesion energy change to the elastic energy change is approximately given by

$$\frac{\Delta W_a}{\Delta E_e} \approx 32 \frac{\gamma_s w}{E b^2} \eta^4. \quad (5)$$

When this ratio is large, or when the lamellae are made of soft material with a high surface energy and have a large aspect ratio, the adhesion tends to persist even after the evaporation of liquid film.

For the array of cylindrical pillars, as shown in Fig. 4(b), interactions of four pillars should be taken into account. When the four pillars make a bundle, each pillar contacts two other pillars with deformation of the contact area. The elastic strain energy stored in each pillar,  $E_e \sim \frac{1}{2} E I s^2 y^{-3}$ . The elastic energy decrease with the increase of the non-contact length by  $\Delta y$  is given by  $\Delta E_e \sim 3 E I s^2 \Delta y / (2y^4)$ . The adhesion energy changes as the pillars become separated, which consists of the energy increase associated with creation of new surfaces ( $4\gamma_s w_c$ ) and the energy decrease due to restoration of surfaces deformed over the contact region. We assume that the contact width  $w_c$  of the four-pillar bundle can be estimated by considering the contact of two identical cylinders as determined by the JKR (Johnson-Kendall-Roberts) theory using a balance between the surface and elastic energies:<sup>35,36</sup>  $w_c \sim 4[d^2 \gamma_s / (\pi E)]^{1/3}$ . It can be shown that the energy decrease associated with restoration of deformed surfaces of two identical cylinders upon separation (per unit height) is given by  $\gamma_s w_c / 2$ .<sup>37</sup> Then the adhesion energy change of a pillar in the four-pillar bundle becomes  $\Delta W_a \approx 3\gamma_s w_c \Delta y$ . We should get  $\Delta E_e > \Delta W_a$  or  $\Delta W_a / \Delta E_e < 1$  for the system to be separated. The



ratio of the adhesion energy change to the elastic energy change for cylindrical pillars is scaled as

$$\frac{\Delta W_a}{\Delta E_e} \approx \frac{128}{\pi} \frac{\gamma_s w_c}{E s^2} \eta^4. \quad (6)$$

As the ratio of (5) does for the lamellae, the energy change ratio of (6) quantifies the tendency for the pillar bundles to keep stuck after drying.

To verify the validity of our scaling argument on the conditions for permanent adhesion, we plot the experimental data used in Fig. 3(b) in the two-dimensional space constructed by the energy change ratio and the aspect ratio in Fig. 4(c). The final states of all the patterns considered are correctly predicted by the energy change ratio. In particular, PDMS pillars and lamellae of the aspect ratio  $\eta = 2$ , which are wet by water through air plasma treatment, are eventually separated despite initial coalescence following the identical process to that displayed in Fig. 3(c) (Multimedia view). Because the surface energy of PDMS was temporarily raised by air plasma treatment before contacting water, we waited 72 h with the PDMS patterns immersed in water until its surface energy returns to the intrinsic value (22 mJ/m<sup>2</sup>), and then let the patterns dry.

Although the energy change ratio determines the eventual state of the patterns, the moment ratio considered above still plays an important role in the clustering of pillars. If the capillary moments, a function of liquid surface tension and contact angle as well as pattern dimension, are not large enough to pull the patterns together, the adhesion between the contacting surfaces cannot happen. To deter pattern stiction, therefore, one needs either to prevent the contact of the patterns when wet by making the moment ratio small or to let the patterns spontaneously separate upon liquid drying by making the energy change ratio small.

## V. CONCLUSIONS

We experimentally visualized and theoretically analyzed the self-organization behavior of slender microstructures like arrays of pillars and lamellae due to liquid evaporation. By considering the capillary moments bending the patterns and elastic resistance, we obtained a moment ratio which can predict whether the patterns would cluster while liquid dries. However, our experiments revealed that the clumped patterns can be restored as the patterns are completely dried in some conditions. We explained this restoration behavior by considering the change of adhesion and elastic energy of the system. We find that the capillary forces must be large enough to overcome the elastic resistance to pull the patterns together, but it is the surface energy of solid patterns that maintains their permanent stiction.

In actual semiconductor manufacturing processes, lowering the moment ratio becomes extremely difficult because of the constraint in available rinse liquids and ever-increasing trend of the aspect ratio.<sup>20</sup> Although use of supercritical fluids with no surface tension can solve the problem, difficulties and costs in raising the temperature and pressure to achieve the supercritical state prevent it from being adopted by industry easily. Thus, if it is ever impossible to prevent initial contact of patterns due to capillary effects, lowering the energy change ratio to induce pattern restoration in the final stage can be a viable solution to the pattern stiction problem. Furthermore, our experimental finding that the array base is dried first rather than the upper portion of the microstructures can lead to a novel process design which can control the liquid film behavior to reduce pattern deformation.

## ACKNOWLEDGMENTS

This work was supported by National Research Foundation of Korea (Grant Nos. 2014023206, 2015035006, and 2014048162) via SNU-IAMD.

<sup>1</sup> H.-Y. Kim and L. Mahadevan, "Capillary rise between elastic sheets," *J. Fluid Mech.* **548**, 141-150 (2006).

<sup>2</sup> A. D. Gat and M. Gharib, "Elasto-capillary coalescence of multiple parallel sheets," *J. Fluid Mech.* **723**, 692-705 (2013).

<sup>3</sup> Z. Wei, T. M. Schneider, J. Kim, H.-Y. Kim, J. Aizenberg, and L. Mahadevan, "Elastocapillary coalescence of plates and pillars," *Proc. R. Soc. A* **471**, 20140593 (2015).

<sup>4</sup> C. Py, P. Reverdy, L. Doppler, J. Bico, B. Roman, and C. N. Baroud, "Capillary origami: Spontaneous wrapping of a droplet with an elastic sheet," *Phys. Rev. Lett.* **98**, 156103 (2007).

- <sup>5</sup> J. Huang, M. Juskiewicz, W. H. de Jeu, E. Cerda, T. Emrick, N. Menon, and T. P. Russell, "Capillary wrinkling of floating thin polymer films," *Science* **317**, 650-653 (2007).
- <sup>6</sup> D. Vella, M. Adda-Bedia, and E. Cerda, "Capillary wrinkling of elastic membranes," *Soft Matter* **6**, 5778-5782 (2010).
- <sup>7</sup> K. J. Park and H.-Y. Kim, "Bending of floating flexible legs," *J. Fluid Mech.* **610**, 381-390 (2008).
- <sup>8</sup> D. Vella, "Floating objects with finite resistance to bending," *Langmuir* **24**, 8701-8706 (2008).
- <sup>9</sup> L. J. Burton and J. W. M. Bush, "Can flexibility help you float?," *Phys. Fluids* **24**, 101701 (2012).
- <sup>10</sup> H. J. Lee, Y. S. Chang, Y. P. Lee, K.-H. Jeong, and H.-Y. Kim, "Deflection of microcantilever by growing vapor bubble," *Sens. Actuators, A* **136**, 717-722 (2007).
- <sup>11</sup> J. Bico, B. Roman, L. Moulin, and A. Boudaoud, "Elastocapillary coalescence in wet hair," *Nature* **432**, 690 (2004).
- <sup>12</sup> N. Chakrapani, B. Wei, A. Carrillo, P. M. Ajayan, and R. S. Kane, "Capillarity-driven assembly of two-dimensional cellular carbon nanotube foams," *Proc. Natl. Acad. Sci. U. S. A.* **101**, 4009-4012 (2004).
- <sup>13</sup> B. Pokroy, A. K. Epstein, M. Persson-Gulda, and J. Aizenberg, "Fabrication of bioinspired actuated nanostructures with arbitrary geometry and stiffness," *Adv. Mater.* **21**, 463-469 (2009).
- <sup>14</sup> B. Pokroy, S. H. Kang, L. Mahadevan, and J. Aizenberg, "Self-organization of a mesoscale bristle into ordered, hierarchical helical assemblies," *Science* **323**, 237-240 (2009).
- <sup>15</sup> H. Duan and K. K. Berggren, "Directed self-assembly at the 10 nm scale by using capillary force-induced nanocoherence," *Nano Lett.* **10**, 3710-3716 (2010).
- <sup>16</sup> M. Fusi, F. Di Fonzo, C. Casari, E. Maccallini, T. Caruso, R. Agostino, C. Bottani, and A. Li Bassi, "Island organization of TiO<sub>2</sub> hierarchical nanostructures induced by surface wetting and drying," *Langmuir* **27**, 1935-1941 (2011).
- <sup>17</sup> T. Tanaka, M. Morigami, and N. Atoda, "Mechanism of resist pattern collapse during development process," *Jpn. J. Appl. Phys., Part 1* **32**, 6059-6064 (1993).
- <sup>18</sup> T. Abe, W. C. Messner, and M. L. Reed, "Effects of elevated temperature treatments in microstructure release procedure," *J. Microelectromech. Syst.* **4**, 66-75 (1995).
- <sup>19</sup> H.-M. Kwon, H.-Y. Kim, J. Puell, and L. Mahadevan, "Equilibrium of an elastically confined liquid drop," *J. Appl. Phys.* **103**, 093519 (2008).
- <sup>20</sup> G. H. Kim, S. H. Cho, J. H. Han, Y. B. Lee, C. H. Roh, K. Hong, and S. K. Park, "Effect of drying liquid on stiction of high aspect ratio structures," *Solid State Phenom.* **187**, 75-78 (2012).
- <sup>21</sup> K. Singh, J. R. Lister, and D. Vella, "A fluid-mechanical model of elastocapillary coalescence," *J. Fluid Mech.* **745**, 621-646 (2014).
- <sup>22</sup> M. Taroni and D. Vella, "Multiple equilibria in a simple elastocapillary system," *J. Fluid Mech.* **712**, 273-294 (2012).
- <sup>23</sup> Y.-H. Yeh, K.-H. Cho, and L.-J. Chen, "Effects of softness of polydimethylsiloxane on the hydrophobicity of pillar-like patterned surfaces," *Soft Matter* **8**, 1079-1086 (2012).
- <sup>24</sup> K. Kendall, "Adhesion: Molecules and mechanics," *Science* **263**, 1720-1725 (1994).
- <sup>25</sup> K. Deguchi, K. Miyoshi, T. Ishii, and T. Matsuda, "Patterning characteristics of a chemically-amplified negative resist in synchrotron radiation lithography," *Jpn. J. Appl. Phys., Part 1* **31**, 2954-2958 (1992).
- <sup>26</sup> T. Tanaka, M. Morigami, H. Oizumi, T. Soga, T. Ogawa, and F. Murai, "Prevention of resist pattern collapse by resist heating during rinsing," *J. Electrochem. Soc.* **141**, L169-L171 (1994).
- <sup>27</sup> D. Chandra and S. Yang, "Stability of high-aspect-ratio micropillar arrays against adhesive and capillary forces," *Acc. Chem. Res.* **43**, 1080-1091 (2010).
- <sup>28</sup> S. P. Timoshenko and J. N. Goodier, *Theory of Elasticity* (McGraw-Hill, New York, 1970).
- <sup>29</sup> M. K. Chaudhury and G. M. Whitesides, "Direct measurement of interfacial interactions between semispherical lenses and flat sheets of poly (dimethylsiloxane) and their chemical derivatives," *Langmuir* **7**, 1013-1025 (1991).
- <sup>30</sup> J. Bauer, G. Drescher, and M. Illig, "Surface tension, adhesion and wetting of materials for photolithographic process," *J. Vac. Sci. Technol., B* **14**, 2485-2492 (1996).
- <sup>31</sup> F. Schneider, T. Fellner, J. Wilde, and U. Wallrabe, "Mechanical properties of silicones for MEMS," *J. Micromech. Microeng.* **18**, 065008 (2008).
- <sup>32</sup> C. Hui, A. Jagota, Y. Lin, and E. Kramer, "Constraints on microcontact printing imposed by stamp deformation," *Langmuir* **18**, 1394-1407 (2002).
- <sup>33</sup> T. W. Lee, O. Mitrofanov, and J. W. Hsu, "Pattern-transfer fidelity in soft lithography: The role of pattern density and aspect ratio," *Adv. Funct. Mater.* **15**, 1683-1688 (2005).
- <sup>34</sup> Y. Zhang, C.-W. Lo, J. A. Taylor, and S. Yang, "Replica molding of high-aspect-ratio polymeric nanopillar arrays with high fidelity," *Langmuir* **22**, 8595-8601 (2006).
- <sup>35</sup> C. Hui, Y. Lin, J. Baney, and A. Jagota, "The accuracy of the geometric assumptions in the JKR (Johnson-Kendall-Roberts) theory of adhesion," *J. Adhes. Sci. Technol.* **14**, 1297-1319 (2000).
- <sup>36</sup> K. Johnson, K. Kendall, and A. Roberts, "Surface energy and the contact of elastic solids," *Proc. R. Soc. London, Ser. A* **324**, 301-313 (1971).
- <sup>37</sup> N. J. Glassmaker, A. Jagota, C.-Y. Hui, and J. Kim, "Design of biomimetic fibrillar interfaces: 1. Making contact," *J. R. Soc., Interface* **1**, 23-33 (2004).